


Disruption of GPSM1/CSF1 signaling reprograms tumor-associated macrophages to overcome anti-PD-1 resistance in colorectal cancer

Yang Chen ¹, Huiqing Jia,² Xiangyan Zhang,² Han Zhao,² Yujing Xiao,² Na Li,² Yifan Yao,² Xiaoming Xing¹

To cite: Chen Y, Jia H, Zhang X, et al. Disruption of GPSM1/CSF1 signaling reprograms tumor-associated macrophages to overcome anti-PD-1 resistance in colorectal cancer. *Journal for ImmunoTherapy of Cancer* 2025;**13**:e010826. doi:10.1136/jitc-2024-010826

► Additional supplemental material is published online only. To view, please visit the journal online (<https://doi.org/10.1136/jitc-2024-010826>).

YC and HJ contributed equally.

Accepted 10 February 2025



© Author(s) (or their employer(s)) 2025. Re-use permitted under CC BY-NC. No commercial re-use. See rights and permissions. Published by BMJ Group.

¹The Affiliated Hospital of Qingdao University, Qingdao, Shandong, China

²Department of Pathology, The Affiliated Hospital of Qingdao University, Qingdao, Shandong, China

Correspondence to

Professor Xiaoming Xing; xiaoming.xing@qdu.edu.cn

ABSTRACT

Background Immune checkpoint blockade (ICB) therapies, particularly anti-PD-1, benefit only a limited subset of colorectal cancer (CRC) patients. G-protein signaling modulator 1 (GPSM1) is implicated in immunity and oncology, yet its role in regulating the CRC tumor microenvironment (TME) and contributing to anti-PD-1 resistance remains poorly understood.

Methods We employed single-cell RNA sequencing and multiplex immunofluorescence on tumor samples from anti-PD-1-resistant CRC patients to evaluate GPSM1 expression and its impact on macrophage polarization. An orthotopic CRC xenograft model in C57BL/6 mice was used to assess the role of GPSM1 in vivo. An in vitro co-culture system, alongside mass cytometry and flow cytometry, explored GPSM1's biological functions within the TME. We further used ChIP-PCR, mass spectrometry, and co-immunoprecipitation to elucidate the mechanisms regulating GPSM1 activity.

Results GPSM1 expression was significantly elevated in anti-PD-1-resistant CRC tissues. Enhanced GPSM1 levels promoted anti-PD-1 resistance by driving macrophage polarization toward an immunosuppressive M2 phenotype, facilitating their infiltration into the TME. We identified the deubiquitinase USP9X as a key factor preventing GPSM1 degradation through K63-polyubiquitination. This stabilization of GPSM1 led to MEIS3 nuclear translocation, activating macrophage colony-stimulating factor expression. Importantly, ruxolitinib emerged as a promising GPSM1-targeting candidate, demonstrating improved efficacy in combination with anti-PD-1 therapy in both microsatellite instability-high and microsatellite stable CRC models.

Conclusions Our findings highlight the pivotal role of GPSM1-driven M2 macrophage infiltration in mediating anti-PD-1 resistance in CRC. Targeting GPSM1 offers a novel therapeutic strategy to enhance ICB efficacy, potentially broadening the patient population that may benefit from these therapies.

INTRODUCTION

Colorectal cancer (CRC) ranks among the most prevalent cancers globally.¹ Despite advancements in chemotherapy and immunotherapy, the mortality rate remains high,

WHAT IS ALREADY KNOWN ON THIS TOPIC

⇒ In colorectal cancer (CRC), immune checkpoint blockade (ICB) therapies, particularly anti-PD-1, have shown limited success, with only a subset of patients responding. Tumor-associated macrophages (TAMs) are known to contribute to an immunosuppressive tumor microenvironment (TME) that supports immune evasion and therapy resistance. G-protein signaling modulator 1 (GPSM1) has been implicated in various immune functions, but its role in regulating macrophage polarization and its contribution to anti-PD-1 resistance in CRC have not been well defined. Understanding the mechanisms by which GPSM1 influences TAM activity and ICB resistance is crucial for developing more effective therapies for CRC.

primarily due to tumor metastasis and recurrence.^{2,3} Immune checkpoint blockade (ICB) therapies, such as anti-PD-1 reagents, have revolutionized cancer treatment.⁴ However, in CRC, the response is largely limited to a small subset of patients with microsatellite instability-high (MSI-H) or deficient mismatch repair (MMR), due to low tumor mutational burden (TMB) and a scarcity of tumor-infiltrating lymphocytes.^{5,6} Therefore, it is essential to understand the molecular mechanisms underlying immune evasion in CRC and develop novel therapeutic strategies to enhance the effectiveness of immunotherapies for patients with proficient MMR, MSI-low, or microsatellite stable (MSS) CRC.

G-protein-signaling modulator 1 (GPSM1), a member of the G-protein signaling regulatory family, interacts with the G-protein alpha subunit, altering its conformation and either activating or inhibiting G-protein signaling.⁷ The role of GPSM1 in tumors is still under debate, as it has been reported to act as either an oncogene^{8,9} or a tumor suppressor.¹⁰ Our previous study identified GPSM1 as a key

WHAT THIS STUDY ADDS

⇒ Our results showed that elevated GPSM1 expression in CRC promoted anti-PD-1 resistance by driving macrophage polarization toward the immunosuppressive M2 phenotype. This polarization facilitated macrophage infiltration into the TME, contributing to immune evasion. We identified USP9X as a key factor preventing GPSM1 degradation via K63-polyubiquitination, which stabilized GPSM1 and triggered MEIS3 nuclear translocation, subsequently activating colony-stimulating factor expression. Targeting GPSM1 with ruxolitinib, in combination with anti-PD-1 therapy, significantly improved antitumor efficacy in both microsatellite instability-high and microsatellite stable CRC models. This highlights GPSM1 as a potential therapeutic target to overcome resistance to ICB in CRC.

HOW THIS STUDY MIGHT AFFECT RESEARCH, PRACTICE OR POLICY

⇒ Based on this study, we explored the regulatory role of GPSM1 in the tumor immune microenvironment of CRC, particularly focusing on its contribution to anti-PD-1 resistance through macrophage polarization. These findings deepen our understanding of the mechanisms underlying immune evasion in CRC, specifically the role of TAMs in promoting immunosuppressive environments. This research provides a novel perspective for enhancing immunotherapy efficacy. Targeting GPSM1, especially in combination with anti-PD-1 therapies, could be a promising strategy to overcome resistance and broaden the range of patients benefiting from ICB.

gene promoting CRC metastasis through the inhibition of autophagy and the activation of the PI3K/AKT/mTOR signaling pathway.¹¹ Studies have shown that the activation of G-protein alpha subunit signaling is a crucial factor leading to the dysfunction of immune effector T cells and the failure of immunotherapy in cancers such as breast cancer, liver cancer, and melanoma.¹² Furthermore, recent investigations show that targeting the homologous protein of GPSM1 and RGS1, in combination with CAR-T therapy and anti-PD-L1 drugs, significantly enhances effector T cell infiltration and decreases tumor volume in breast cancer xenograft models.¹³ However, few researchers explored the potential role of GPSM1 in modulating the tumor microenvironment (TME). It is still unclear whether GPSM1 can influence immune cell functions and thus affect the efficacy of immune checkpoint inhibitors in CRC patients.

Tumor-associated macrophages (TAMs), a key component of immune cells within the TME,¹⁴ constitute up to half of the cells in TME and are generally linked to poorer prognosis in CRC patients.¹⁵ TAMs often exhibit M2-like macrophage characteristics and participate directly or indirectly in tumor progression. Given that TAMs are a dynamic cell population,¹⁶ redirecting them toward an antitumor phenotype may offer an opportunity to reconfigure the immunosuppressive TME and enhance the efficacy of ICB therapy.¹⁷ Although recent advances have been made in preclinical and clinical studies,¹⁸ some questions remain unanswered. Therefore, elucidating the precise mechanisms of M2-like macrophage polarization

could aid in the discovery of effective and promising immunotherapies for tumors.

In this study, we revealed that GPSM1-driven M2 macrophage infiltration played a pivotal role in mediating resistance to anti-PD-1 therapy in CRC. We identified GPSM1 as a significant predictor of anti-PD-1 therapy response. Moreover, our findings demonstrated that the deubiquitinase USP9X safeguarded GPSM1 from degradation in CRC by removing its K63-linked polyubiquitin chains. This stabilization of GPSM1 enhanced the nuclear translocation of MEIS3 through clathrin-mediated endocytosis, which in turn facilitated the transcriptional activation of colony-stimulating factor (CSF1), leading to increased macrophage recruitment and the M2-like polarization of macrophages in CRC. Furthermore, our results indicated that targeting the GPSM1 pathway might amplify the therapeutic effects of anti-PD1 therapy, offering a potential combination therapy strategy based on GPSM1 expression in CRC.

MATERIALS AND METHODS

Animal experiments

Female C57BL/6J, nude, and BALB/C mice, aged 6–8 weeks, were procured from the Vital River Laboratory Animal Technology (Beijing, China) and housed in a barrier facility under strictly controlled environmental conditions, including temperature (18°C–22°C), humidity (50%–60%), and light/dark cycle (12 hours).

Human samples and cell culture

This study included two cohorts of CRC patients:

Cohort 1: From 2016 to 2018, 126 paraffin-embedded CRC specimens were collected from patients who underwent radical resection without preoperative therapy at the Affiliated Hospital of Qingdao University. Tissue microarrays (TMAs) were constructed, and immunohistochemical (IHC) staining was performed to assess GPSM1, CD8, CD68, and CD163 expression. Patients ranged in age from 23 to 84 years (median: 64 years) and included 81 males and 45 females. Tumors were primarily located in the rectum (123 cases). Tumor differentiation, staging, MSI status, and neural invasion data are summarized in online supplemental table 7. Median disease-free survival (DFS) was not determined due to limited progression events, and 67.5% of patients were alive at the last follow-up.

Cohort 2: We collected surgical samples from six CRC patients who received anti-PD-1 therapy at our hospital between 2021 and 2023. Based on the iRECIST criteria, clinical experts, pathologists, and radiologists comprehensively evaluated these samples and classified them into a disease response group and a disease progression group. Details of the patients' treatment regimens, pathological information, and progression timelines are provided in online supplemental table 8. Multiplex immunofluorescence staining was performed to analyze GPSM1 expression and its relationship with immune cell infiltration.

Human CRC cell lines (RKO, SW480) and murine CRC cell lines (MC38, CT26) were sourced from the Committee of Type Culture Collection of the Chinese Academy of Sciences (Shanghai, China). Additionally, human monocytic leukemia THP-1 cells and human embryonic kidney 293T (HEK293T) cells were purchased from the Shanghai Cancer Institute (Shanghai, China). RKO and SW480 cell lines were maintained in DMEM with 10% fetal bovine serum, 100 units/mL penicillin, and 100 µg/mL streptomycin. MC38 and CT26 cell lines were cultured in RPMI-1640 medium supplemented with 10% fetal bovine serum, 100 units/mL penicillin, and 100 µg/mL streptomycin.

Macrophage preparation and polarization

THP-1 cells were cultured in RPMI 1640 medium with 50 ng/mL PMA (Sigma, USA) for 48 hours to generate M0 macrophages. After a 24-hour rest period, M0 cells were treated with 100 ng/mL LPS (Sigma, USA) and 20 ng/mL IFN-γ (PeproTech, USA) to induce M1-like macrophages, or with 20 ng/mL IL-4 (PeproTech, USA) to induce M2-like macrophages.

RNA extraction and quantitative PCR

Total RNA was isolated using the RNAiso Plus kit (Cat#9109, Takara, Japan). cDNA was synthesized using a reverse transcription kit (Cat#R232-01, Vazyme, Nanjing, China). Quantitative PCR (qPCR) was performed using a LightCycler 480 system (Roche, USA) and SYBR qPCR Master Mix (Cat#MQ101-01, Vazyme, Nanjing, China). Gene expression was normalized to GAPDH using the $\Delta\Delta C_t$ method. Primer sequences are detailed in online supplemental table 5.

Immunohistochemistry

IHC was conducted on formalin-fixed, paraffin-embedded CRC tissue sections. Sections were deparaffinized, rehydrated, and subjected to heat-induced epitope retrieval using citrate buffer (pH 6.0). Endogenous peroxidase activity was blocked with 3% hydrogen peroxide. The sections were incubated overnight at 4°C with primary antibodies (details are provided in online supplemental table 6) diluted as per the manufacturer's instructions. Staining was visualized using a DAB kit (Gene Tech, Shanghai, China) and counterstained with hematoxylin. Staining evaluation was performed by two independent pathologists who were blinded to the clinical data.

Cytoplasmic GPSM1 expression was evaluated and scored by two pathologists independently, both blinded to the clinical diagnosis. The scoring system calculated the score using both the percentage of positive tumor cells and the staining intensity. The percentage of positive cells was scored as follows: 0 for negative staining, 1 for 1%–25%, 2 for 26%–50%, 3 for 51%–75%, and 4 for >75%. Staining intensity was scored on a scale of 0–3 (0: none, 1: weak, 2: moderate, 3: strong). The final GPSM1 expression score was determined by multiplying the two values, resulting in a total score ranging from 0 to 12. A

total score >7 was classified as high GPSM1 expression. For immune cell quantification, CD8+T cells, CD68+macrophages, and CD163+macrophages were counted in five representative high-power fields (400×magnification) per slide. The number of positive cells per field of vision was used to calculate the average.

Immunofluorescence

Cells (5×10⁴ per well) were seeded onto sterilized glass coverslips in 24-well plates and allowed to adhere overnight. Cells were fixed with 4% paraformaldehyde for 15 min, permeabilized with 0.1% Triton X-100 for 10 min, and blocked with 5% bovine serum albumin for 30 min. Primary antibodies (see online supplemental table 6) were applied and incubated overnight at 4°C. Fluorescently labeled secondary antibodies were applied for 1 hour at room temperature, and nuclei were counterstained with DAPI for 10 min. Images were acquired using a fluorescence microscope (Olympus, Japan). Fluorescence cut-off values for GPSM1, MEIS3, CD45, CD8, and CD206 were determined using negative controls (unstained samples and isotype controls) to establish background fluorescence levels. A threshold was set at the mean fluorescence intensity of the negative controls plus 2 SD. Positive staining was defined as fluorescence signals above this threshold.

Western blot

CRC cell lines were seeded at 2×10⁶ cells per well in 6-well plates and cultured to 70%–80% confluency. Cells were lysed in RIPA buffer (Solarbio, China) supplemented with protease and phosphatase inhibitors (MedChemExpress, USA). Protein concentration was measured using a BCA protein assay kit (Beyotime, China). Equal amounts of protein (30 µg per sample) were separated by SDS-PAGE, transferred onto PVDF membranes, and blocked with 5% skim milk for 1 hour. Membranes were incubated overnight at 4°C with primary antibodies (online supplemental table 2), followed by HRP-conjugated secondary antibodies for 1 hour at room temperature. Protein bands were visualized using an ECL substrate and quantified using ImageJ. Experiments were repeated three times independently.

Immunoprecipitation assays

Cell lysates were prepared from 1×10⁷ cells per sample using 500 µL of immunoprecipitation (IP) lysis buffer (Solarbio, China) supplemented with protease and phosphatase inhibitors (MedChemExpress, USA). Protein concentration was quantified using a BCA assay (Beyotime, China). For each IP, 500 µg of total protein was incubated with 2 µg of either anti-Flag or anti-GPSM1 antibodies at 4°C overnight with gentle rotation. Prewashed A/G magnetic beads (40 µL per sample) were then added to the antibody-protein complex and incubated for 6 hours at 4°C. The beads were washed three times with lysis buffer, resuspended in 40 µL of 1×SDS-loading buffer (Beyotime, China), and heated at 95°C for 5 min.

The resulting samples were analyzed by Western blotting as described above. Experiments were performed in triplicate for each condition.

Virtual drug screening

The 3D protein structure of GPSM1 was modeled using Schrödinger software, with hydrogen atoms added and water molecules removed using the Prep Wiz module. The FDA-approved drug library, containing 10,000 small molecules, was screened for drug-likeness based on Lipinski's and Veber rules. LigPrep was used for molecular preparation, setting the protonation state to pH 7.4. Active sites were identified using SiteMap, and potential false positives with PAINS characteristics were filtered out using Canvas V.1.1. ADME properties of the compounds were predicted using QikProp V.3.2 to ensure compliance with Lipinski's and Jorgensen's rules. Redundant compounds were removed through FCFP₆ fingerprint clustering analysis.

Compound library screening

A focused FDA small-molecule inhibitor library containing 87 compounds was purchased from MedChemExpress. CRC cell lines (RKO and SW480) were seeded into 96-well plates at a density of 5000 cells per well in 100 μ L of complete medium. After 24 hours, cells were treated with 2 μ M of each inhibitor for 12 hours. Cell viability was assessed using a CCK-8 assay (Dojindo, Japan) in triplicate for each compound. Results were analyzed to identify compounds that reduced cell viability by more than 50%. Detailed compound information is provided in online supplemental table 9.

ChIP-PCR assay

Cells (1×10^7 per sample) were crosslinked with 1% formaldehyde for 10 min at room temperature, then quenched with 0.125 M glycine for 5 min. After washing with ice-cold PBS, cell pellets were stored at -80°C . Chromatin was prepared by lysing cells in 500 μ L lysis buffer on ice for 10 min, centrifuging at $12,000 \times g$ for 5 min at 4°C , and sonicating (20 cycles, 30 s on/off) to produce 200–500 bp fragments, confirmed by agarose gel electrophoresis. For IP, 5 μ g of specific antibody (eg, anti-Flag) or IgG control was conjugated to Protein A/G magnetic beads overnight at 4°C . Sheared chromatin (50 μ L, $\sim 2 \times 10^6$ cells) was incubated with antibody-bound beads at 4°C overnight. Beads were washed with sequential low-salt, high-salt, and LiCl buffers, and protein-DNA complexes were eluted. Cross-links were reversed at 65°C for 6 hours, followed by RNase A and proteinase K treatments. DNA was purified using phenol-chloroform extraction or a column-based kit. qPCR was performed in triplicate with primers targeting specific regions, using 1% input DNA as a normalization control.

Tissue dissociation and single-cell suspension preparation

Tumor tissues from NC (normal control) and GPSM1-overexpressing orthotopic CRC mouse models were collected, washed with ice-cold PBS, and minced into

1–2 mm³ pieces. These were incubated in GEXSCOPE tissue dissociation solution (Singleron) for 15 min at 37°C to generate single-cell suspensions. The digested mixture was filtered through a 70 μ m strainer, centrifuged, and resuspended in PBS. Red blood cells were removed using GEXSCOPE erythrocyte lysis buffer. The final cell suspension was assessed for viability using trypan blue and adjusted to a concentration of 1×10^5 cells/mL. Single-cell RNA libraries were prepared using the GEXSCOPE Single-Cell RNA Library Kit (Singleron) and sequenced on the Illumina HiSeq X platform.

Single-cell transcriptional program feature gene analysis and signature quantification

All additional analyses were conducted using R V.4.3.0. Unsupervised clustering and integration were performed with Seurat and Harmony. Highly variable genes were used for PCA, and the top 30 principal components were used for UMAP and t-SNE visualization. Differentially expressed genes for each subcluster were identified with Seurat's "FindAllMarkers," and cell types were annotated based on canonical marker genes. Transcription factor activity was analyzed with the R package DoRothEA. To study GPSM1-high tumor cell interactions with CCL8+macrophage cells, we used ALRA for imputation, and CellPhoneDB for interaction inference.

Database analysis

The single-cell RNA sequencing data are available from the CNGB database (accession number CNP0006600).¹⁹ The immune infiltration data of COAD and READ were obtained from TIMER 2.0.²⁰

Statistical analysis

Statistical analyses were performed using SPSS (V.26) and GraphPad Prism V.9. Data are presented as the mean \pm SD. Differences between two independent groups were assessed using an unpaired Student's t-test. For comparisons involving three or more groups, a one-way analysis of variance was used. Correlation analyses were conducted using Pearson's correlation test. Survival analysis was performed using Kaplan-Meier curves with log-rank testing.

RESULT

GPSM1 mediates immune suppression in CRC mice models

We performed a detailed analysis of the pathological characteristics of CRC tissues with elevated GPSM1 expression in cohort 1. We found that tissues with high GPSM1 levels exhibited limited immune cell infiltration and predominantly displayed the MSS phenotype (online supplemental table 1), which is typically the phenotype resistant to ICB. To examine the role of GPSM1 in antitumor immunity, we established two distinct mouse models using MC38 cells: immune-competent C57BL/6 mice and immune-deficient BALB/c nude mice, both with lentivirus-mediated GPSM1 overexpression. The results

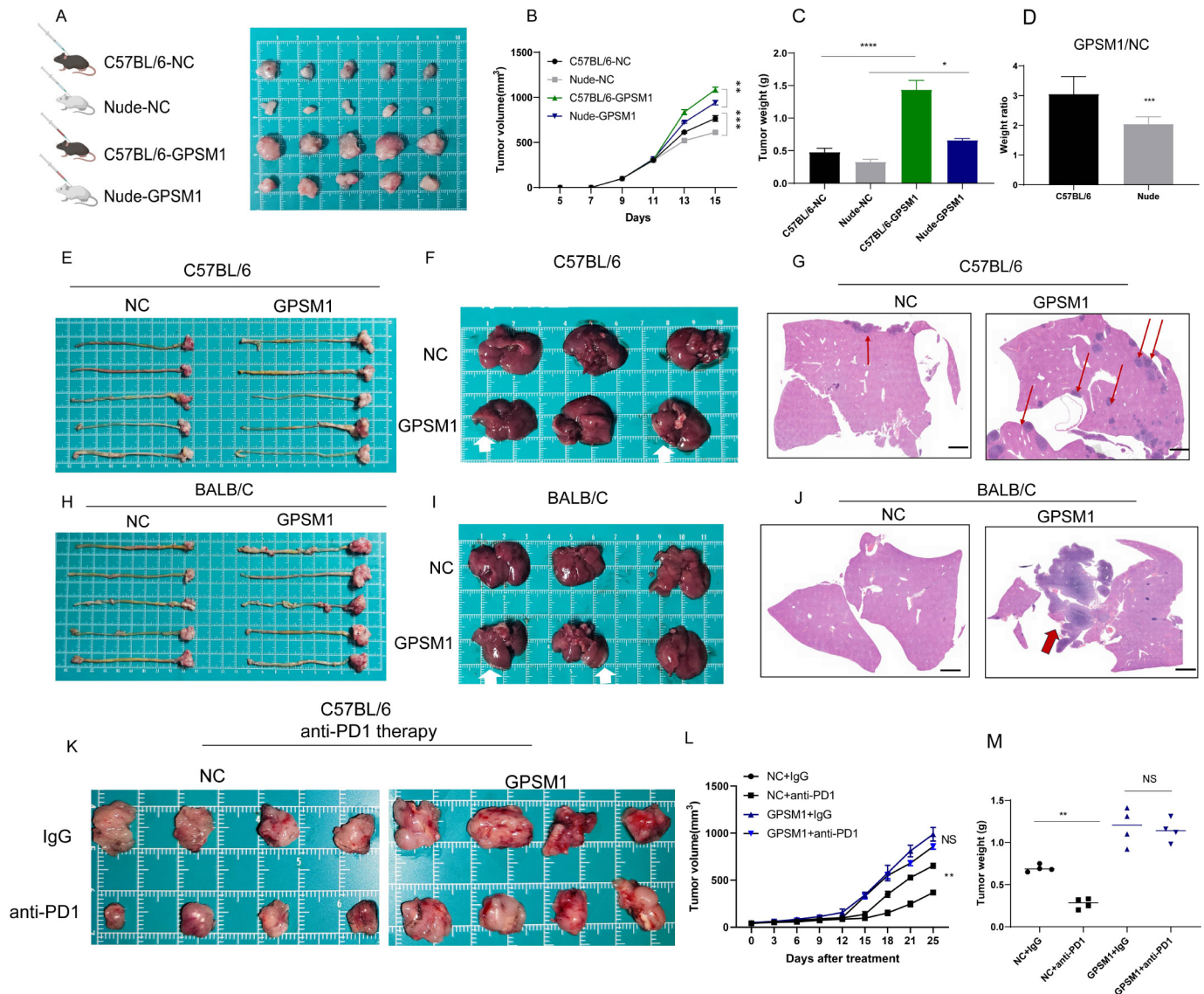


Figure 1 GPSM1 overexpression promotes colorectal tumor growth, metastasis, and response to anti-PD-1 therapy in murine models (A) Immunocompetent C57BL/6 mice and immune nude mice were subcutaneously inoculated with MC38-NC or MC38-GPSM1. Mice were sacrificed when tumor volumes reached a threshold of 1500 mm³. (B–D) Tumor volume and weight in MC38 xenografts with GPSM1 overexpression showed significantly increased growth compared with their respective controls. (E–G) Establishment of an orthotopic colorectal cancer model in C57BL/6 mice using MC38 cells overexpressing GPSM1. (E) Comparison of tumor size differences between the GPSM1-overexpressing group and the control group in the intestine. (F) Differences in liver metastasis between the GPSM1-overexpressing group and the control group (metastatic nodules indicated by white arrows). (G) HE staining images of liver tissue from the NC group and the GPSM1 group (metastatic nodules indicated by red arrows). Scale bar: 50 μm. (H–J) Establishment of an orthotopic colorectal cancer model in BALB/c using CT26 cells overexpressing GPSM1. (H) Comparison of tumor size differences between the GPSM1-overexpressing group and the control group in the intestine. (I) Differences in liver metastasis between the GPSM1-overexpressing group and the control group (metastatic nodules indicated by white arrows). (J) HE staining images of liver tissue from the NC group. (L) HE staining images of liver tissue from the GPSM1 group (metastatic nodules indicated by red arrows). Scale bar: 50 μm. (K) Isotype control (IgG) or anti-mouse PD-1 antibody were given at 200 μg/mouse on days 4, 7, and 9 post cell injection, and representative images of tumors from each group were shown. (L, M) The weight of the orthotopic colorectal tumors and the body weight of the mice in different groups. $p < 0.05$; $** p < 0.01$; $*** p < 0.001$; $**** p < 0.0001$. Statistical significance was determined using [insert method, e.g., Student's t-test, ANOVA].

demonstrated that GPSM1 overexpression significantly accelerated tumor growth in C57BL/6 mice compared with BALB/c nude mice (figure 1A–D). Orthotopic xenograft models in C57BL/6 and BALB/c mice further indicated that GPSM1 overexpression led to faster tumor

growth and a higher incidence of distant liver metastasis compared with the control group (figure 1E–J). We, therefore, hypothesized that GPSM1's tumor-promoting effects are at least partially dependent on a functional immune system. Further, we examined the potential role of GPSM1

in ICB resistance in CRC by administering anti-PD1 treatment to mice overexpressing GPSM1 (figure 1K). The GPSM1-control group exhibited a significant reduction in tumor burden compared with the vehicle group. However, in the GPSM1-overexpressing groups, no significant difference was observed (figure 1L,M). These findings suggested that GPSM1 might be a key gene driving resistance to anti-PD1 therapy by modulating the TME in CRC.

GPSM1 overexpression promoted an immunosuppressive TME and contributed to resistance to anti-PD-1 therapy in CRC

To investigate the impact of GPSM1 overexpression on the TME, we performed single-cell sequencing on 62,795 cells from tumor tissues of the orthotopic CRC mouse model (NC*3: 29,415 vs GPSM1*3: 33,380) (figure 2A), identified seven major cell types: epithelial cells, endothelial cells, fibroblasts, T and NK cells, neutrophils, mononuclear phagocytes, and red blood cells through unsupervised clustering and manual annotation (online supplemental figure 1A). Further, we conducted an in-depth UMAP dimensionality reduction analysis on the abundant T and NK cells, from which we identified two NK cell populations (NK, NK_T), four CD8+T cell populations (CD8_Proliferating T, CD8_Naive T, CD8_Teff (effector), CD8_Tex (exhausted)), and two CD4+T cell populations (CD4_Naive T, CD4_Treg) (figure 2B,C). After clustering annotation, we detected the difference between the control group and the GPSM1 overexpression group. In tumors with GPSM1 overexpression, the proportion of immunosuppressive cells, such as CD8+exhausted T cells (11.42%) and CD4+regulatory T cells (12.48%), was higher compared with the control group (6.14% and 10.93%, respectively). Meanwhile, antitumor effector cells, including NK cells (10.19%) and CD8+effector T cells (10.54%), were significantly reduced compared with the control group (17.22% and 26.50%, respectively) (figure 2D, online supplemental table 2). These findings suggest that GPSM1 overexpression alters the tumor immune microenvironment, reducing effector cell infiltration and enriching immunosuppressive populations, thereby promoting immune evasion and resistance to ICIs. Further analysis of TIMER 2.0 data also showed that GPSM1 expression in CRC was negatively correlated with immune effector cells CD4, while positively correlated with immune suppressor cells Treg and exhausted CD8 cells in CRC (figure 2G).

In the single-cell sequencing data, we identified six distinct macrophage clusters (Mac_H2afz, Mac_Ifit2, Mac_Ccl8, Mac_Mmp12, Mac_Rps27, Mac_Mki67) (figure 2E, online supplemental figure B, C), with Mac_Ccl8 notably emerging as the predominant population among tumor-infiltrating myeloid cells, exhibiting a significantly higher presence in the GPSM1 overexpression group (51.44%) compared with the control group (18.99%) (online supplemental tables 3 and 4). It also exhibited the highest M2-like macrophage signature score among all TAM populations based on M1/M2 macrophage gene

signatures. (figure 2F). More importantly, GPSM1 expression levels were positively correlated with CD163 (M2 macrophage markers) and negatively correlated with CD8 (T cell markers). In addition, the number of CD68+ (M1 macrophages markers) cells in the high GPSM1 expression group was comparable to that in the low GPSM1 expression group (figure 2I,K,L,M, online supplemental figure 1A–E). These findings indicated that high expression of GPSM1 in CRC might promote the development of an immunosuppressive TME, primarily due to the infiltration of M2-like macrophages. Indeed, we collected samples from patients with disease progression or partial response following anti-PD-1 therapy (cohort 2). Our findings revealed that GPSM1, predominantly localized in the cytoplasm, is more highly expressed in patients with a disease progression to anti-PD-1 treatment compared with those with partial response, while CD45-positive immune cells were decreased in the patients with disease progression (figure 2H,J). Importantly, survival analysis in cohort 1 indicated that high GPSM1 expression was associated with poor DFS. Notably, GPSM1^{high}/CD8^{low}, GPSM1^{high}/CD68^{low} and GPSM1^{high}/CD163^{high} patients experienced poorer DFS than GPSM1^{low}/CD8^{high}, GPSM1^{low}/CD68^{high} and GPSM1^{low}/CD163^{low} patients (online supplemental figure 1D–G). Consequently, GPSM1 plays a pivotal role in contributing to unfavorable prognoses and resistance to anti-PD1 therapy in CRC.

GPSM1 overexpression in CRC cells promoted M2-like macrophage polarization and enhanced PD-L1 expression

To further validate the impact of GPSM1 on macrophages, an in vitro co-culture system was established to facilitate the interaction between CRC cells with varying levels of GPSM1 expression and THP-1 cells (figure 3A,B). Following co-culture with GPSM1-overexpressing CRC cells, macrophages exhibited significantly increased the mRNA and protein levels of M2-like macrophage markers, CD206, ARG-1, IL-10, and TGF- β (figure 3C–H). Flow cytometry revealed that THP-1-differentiated macrophages co-cultured with GPSM1-overexpressing CRC cells displayed a CD206 positive phenotype, which is similar to the phenotype of M2-like macrophages, comparing with those cocultured with the control groups (figure 3I,J). To explore whether GPSM1 affects chemotactic migration of macrophages, we conducted a migration assay using phorbol-12-myristate-13-acetate (PMA)-treated THP-1 cells. As shown in figure 3K,L, the supernatants from the coculture system containing GPSM1 overexpressing CRC cells enhanced the chemotactic migration of macrophages. These findings implied that CRC cells with GPSM1 overexpression enhanced macrophage recruitment and induced M2-like polarization of macrophages in vitro.

In addition, the expression of PD-L1 and the activity of PD-1 checkpoint signaling pathway were involved in biological processes and molecular function of Gene Ontology (GO) analysis, according to the single-cell sequence data analysis of the GPSM1 overexpression

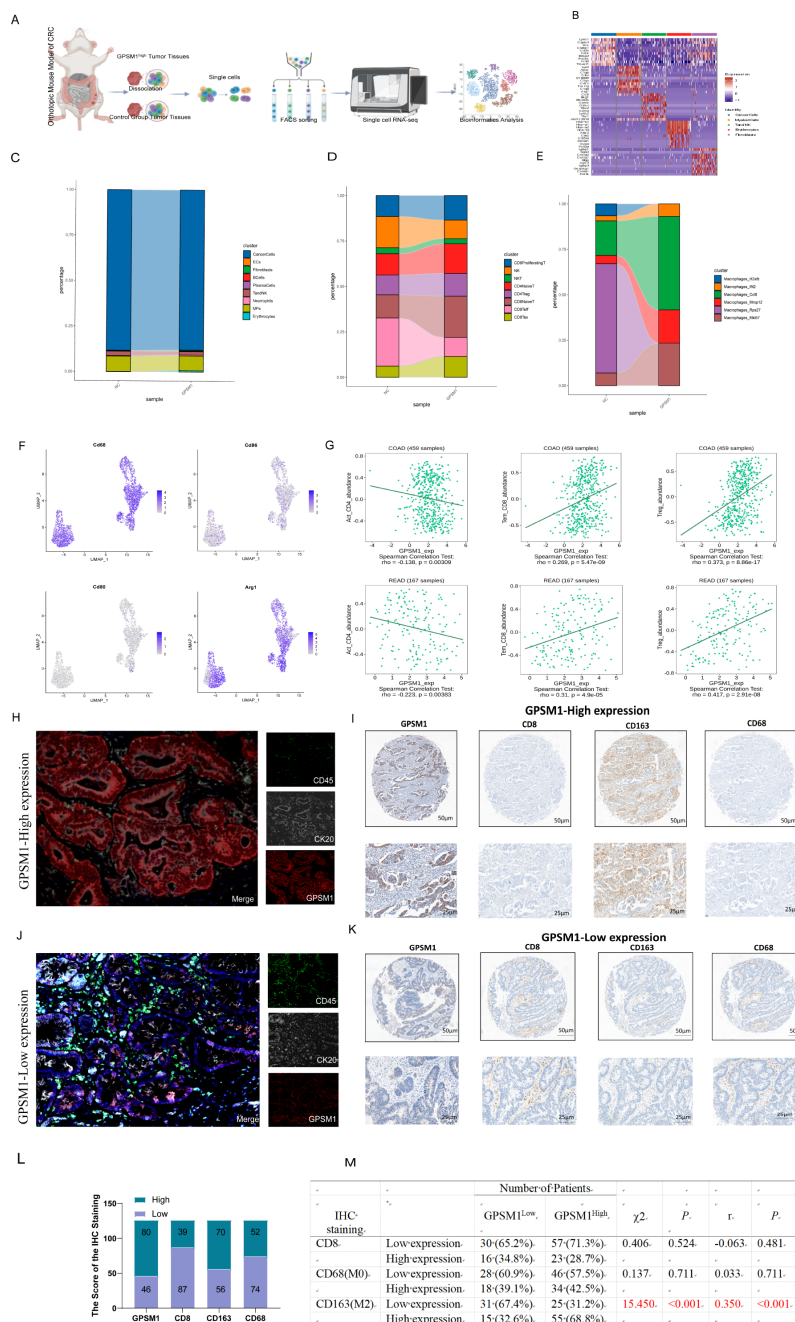
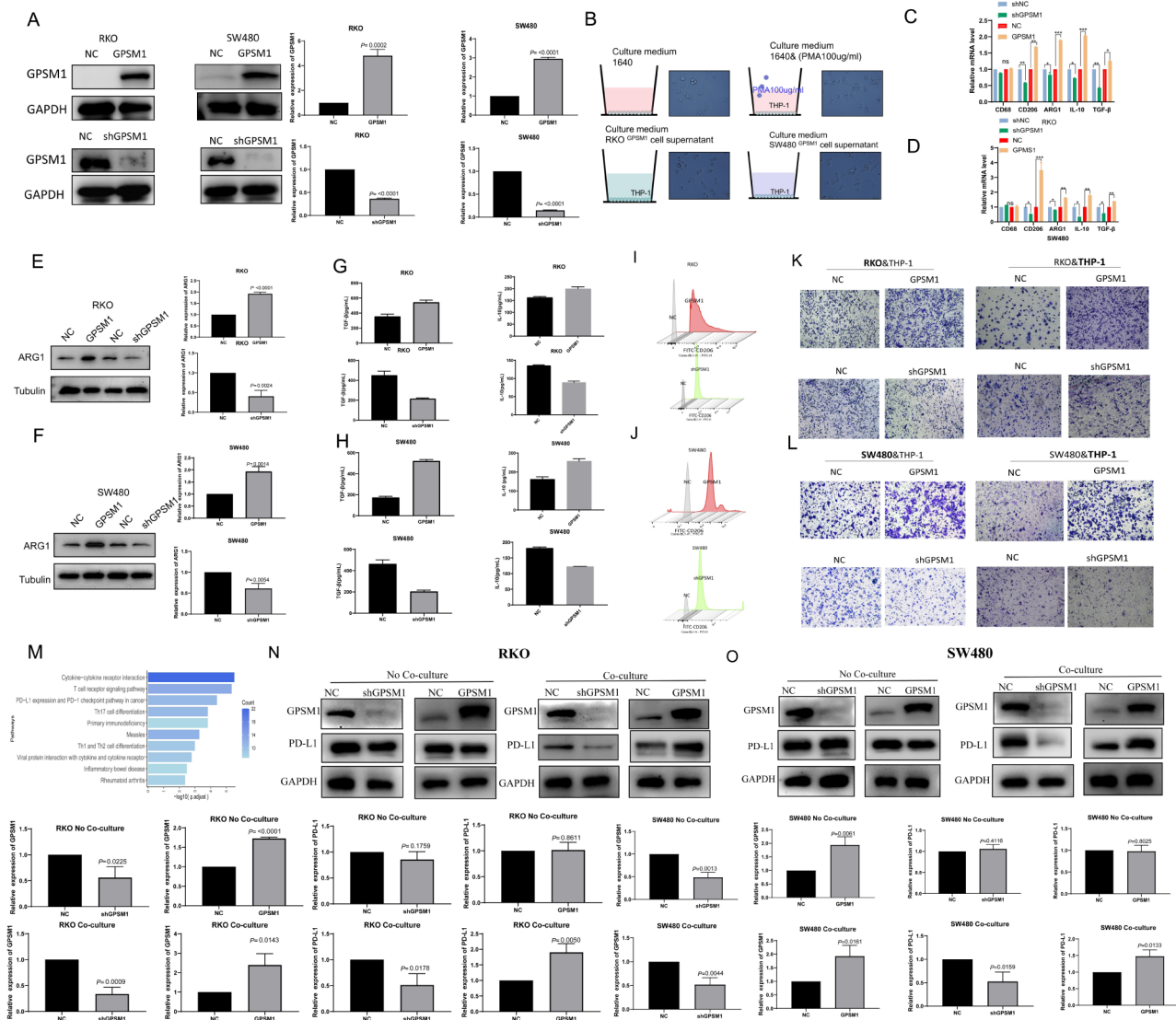


Figure 2 Single-cell profiling of immune cells in GPSM1 high CRC microenvironment. (A) Overview of the experimental design for single-cell RNA sequencing. (B) Uniform manifold approximation (UMAP) plot showing the unsupervised clusters of single cells and annotated cell types. (C) Single-cell transcriptomic landscape of the alteration of cancer cells and main immune lineages in TME of GPSM1-overexpression CRC characterized. (D) Single-cell transcriptomic landscape of the alteration of T and NK cells in TME of GPSM1-overexpression CRC characterized. (E) Single-cell transcriptomic landscape of the alteration of macrophages in TME of GPSM1-overexpression CRC characterized. (F) Characterization of CCL8-macrophage subtypes using macrophage molecular markers: CD68 (M0 macrophage marker), CD86 and CD80 (M1 macrophage markers), and AGR1 (M2 macrophage marker). (G) TIMER2.0 database validation of the correlation between GPSM1 expression and the expression of immune effector cells (CD4) and immunosuppressive cells (Treg and exhausted T cells) in CRC. (H) Representative pictures of immunofluorescence analysis for CD45 (green arrows), CK20 (gray arrows) and GPSM1 (red arrows) in patients with disease progression after anti-PD-1 therapy. Scale bar: 50µm. (I) Representative IHC staining images of GPSM1, CD8 CD163, and CD68 in GPSM1high CRC tissues. Scale bar: 50µm (above) and 25µm (bottom). (J) Presentative pictures of immunofluorescence analysis for CD45 (green arrows), CK20 (gray arrows) and GPSM1 (red arrows) in patients with a partial response to anti-PD-1 treatment. Scale bar: 50µm. (K) Representative IHC staining images of GPSM1, CD8 CD163, and CD68 in GPSM1 low CRC tissues. Scale bar: 50µm (above) and 25µm (bottom). (L) Bar chart showing the number of cases with high and low expression of GPSM1, CD8, CD163, and CD68 in 126 colorectal cancer tissue samples. (M) Correlation analysis between GPSM1 expression levels and immune cell infiltration, including CD8+, CD163+, and CD68+ cells. CRC, colorectal cancer; IHC, immunohistochemical.



cancer cell (figure 3M). Based on the effects of GPSM1 on macrophages, we speculated that GPSM1 might influence PD-L1 expression via macrophages in the CRC microenvironment. Therefore, we evaluated the potential effect of macrophages on the expression of PD-L1 in the coculture system. The result indicated that the PD-L1 expression was significantly higher in GPSM1 expression CRC cells than that in the control group. However, we did not observe significant changes in PD-L1 expression in GPSM1-overexpressing or silencing CRC cells in the non-coculture system (figure 3N,O). Collectively, these findings suggested GPSM1 from CRC cells could induce the formation of the phenotype of M2-like macrophage, which in return promoted the PD-L1 expression in CRC.

GPSM1 promoted macrophage polarization and recruitment via CSF1

To elucidate the cytokines secreted by macrophages that are activated by GPSM1 overexpressing CRC cells, we conducted a ligand-receptor analysis based on single-cell sequence data. The cell-cell communication network identified seven signaling pathways through comparing between tumor cells and Mac_Ccl8, including CD248, VEGFB, VEGFA, LGALS3, IL34, CSF1, and CCL7 (figure 4A). qPCR analysis of these pathways in co-culture systems revealed that the levels of macrophage CSF1 were significantly higher in GPSM1-overexpressing cells with the comparison to control groups (figure 4B,C). Western blot and ELISA further confirmed that CSF1 levels were markedly elevated in the supernatants of RKO-GPSM1 and SW480-GPSM1 CRC cells compared with their counterparts (figure 4D–G).

To investigate the role of CSF1 in the polarization of GPSM1-induced macrophage, we performed a CSF1 rescue experiment using an in vitro co-culture assay. The results demonstrated that knocking down CSF1 expression in GPSM1-overexpressing CRC cells reversed the high expression pattern of M2-like macrophage markers induced by the overexpression of GPSM1 (figure 4H,I,L,M). In contrast, M2-like polarization and macrophage migration were enhanced when cocultured with GPSM1-knockdown CRC cells treated with recombinant CSF1 (rhCSF1) (figure 4J,K,N,O). These findings suggested that CSF1 was likely a critical mediator in GPSM1-induced M2-like macrophage polarization.

GPSM1 enhanced CSF1 expression by promoting the nuclear translocation of MEIS3

To take a deeper look into how GPSM1 regulates CSF1 expression, IP-Mass Spectrometry (IP-MS) was used to identify potential proteins interacting with GPSM1. The silver staining results are displayed in (figure 5A). By cross-referencing the GPSM1-binding proteins identified through MS with the GSEA transcription factor databases, MEIS3 emerged as a crucial transcription factor (figure 5C). The interaction between GPSM1 and MEIS3 was further validated through Co-IP (Co-IP) assays (figure 5D). Previous research has revealed that MEIS3

functions as a transcription factor capable of activating genes including *AcH4*,²¹ *PDX1*,²² and *Cyclin D1*.²³ Next, we knocked down MEIS3 in GPSM1-overexpressing CRC cell lines and observed a corresponding decrease in CSF1 expression (figure 5E). Therefore, we hypothesized that MEIS3 was the key transcription factor regulating CSF1 expression under the control of GPSM1. The MEIS3 motif sequence was identified through a search in the JASPAR database (figure 5F). Consequently, chromatin IP qPCR assays further validated that MEIS3 directly bound to these specific sites on the CSF1 promoter (figure 5F).

Based on the above results, we verified that GPSM1 influenced CSF1 expression through MEIS3. However, it was also very important to investigate the mechanism of GPSM1 affecting MEIS3. As a homeobox transcription factor, MEIS3 must be transported from the cytoplasm to the nucleus to exert its function.²⁴ We further demonstrated that GPSM1 facilitated the translocation of MEIS3 from the plasma membrane to the nucleus (figure 5G,H). GO analysis of the MS results revealed that these molecules were involved in endocytosis, nuclear transport, and export pathways (figure 5I). We further investigated the molecular mechanisms underlying GPSM1-mediated nuclear trafficking. Our result showed that Pitstop, an inhibitor of clathrin-dependent endocytosis, rather than Filipin III, an inhibitor of caveolae-mediated endocytosis, blocked the nuclear localization of MEIS3 (figure 5J,K). This indicated that GPSM1-induced clathrin-dependent endocytosis might facilitate the nuclear translocation of MEIS3.

The deubiquitinase USP9X prevented the degradation of GPSM1 in CRC by deubiquitinating its K63-polyubiquitin chain

Co-IP assays and MS proteomic analysis were conducted to identify proteins interacting with GPSM1 (figure 6A). Notably, USP9X, a well-known deubiquitinase, was identified as a potential binding partner. Previous studies demonstrated that USP9X interacted with the GPR domain of GPSM1 and regulated its expression in specific regions of the rat brain.²⁵ We found that GPSM1 formed a complex with USP9X. In addition, we performed molecular docking analysis, revealing that USP9X has a high affinity to GPSM1. Key binding sites on USP9X, including the amino acid residues Ser1657, Gly1555, and Tyr1968, were identified as potential binding sites for the Tyr305, Gln303, and Leu222 residues on GPSM1 (figure 6B,C).

Subsequently, we treated 293T cells with cycloheximide (CHX) to inhibit protein synthesis and observed that the siRNA-mediated knockdown of USP9X enhanced the degradation of endogenous GPSM1 (figure 6D,E). This led us to hypothesize that USP9X might play a role in regulating the ubiquitin/proteasome pathway. Furthermore, the knockdown of USP9X resulted in a reduction of GPSM1 levels (figure 6F). Notably, treatment with the proteasome inhibitor MG132 significantly rescued the decrease in GPSM1 protein induced by USP9X depletion (figure 6G). Next, to identify the domain of GPSM1 that interacts with USP9X, we designed truncations of various

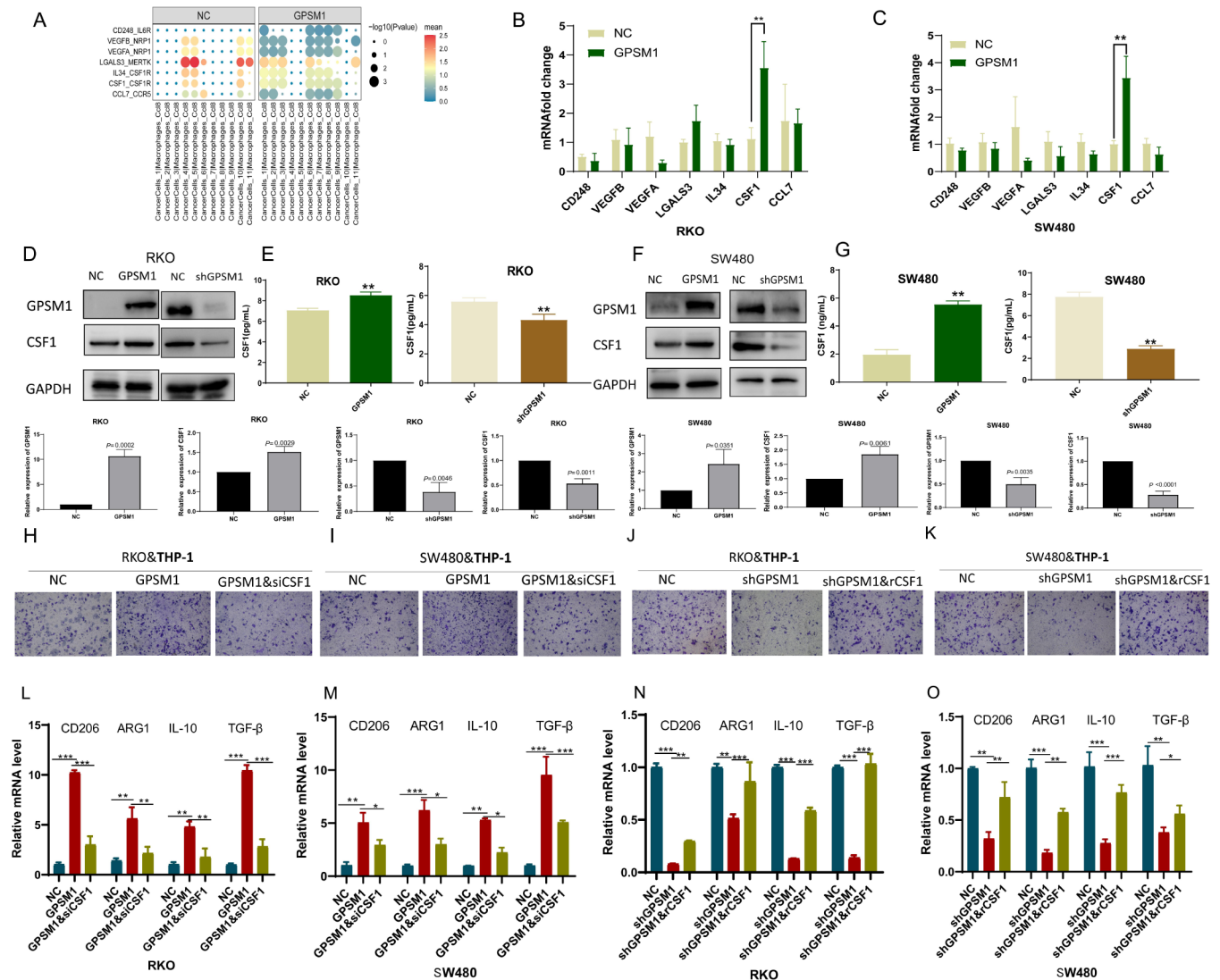


Figure 4 GPSM1 promotes macrophage polarization and recruitment via CSF1. (A) Cell communication analysis of receptor-ligand interactions between CRC cells and CCL8+macrophage populations. (B) qPCR validation of ligand cytokine expression (CD248, VEGFB, VEGFA, LGALS3, IL34, CSF1, and CCL7) in RKO cells within the co-culture system. (C) qPCR validation of ligand cytokine expression (CD248, VEGFB, VEGFA, LGALS3, IL34, CSF1, and CCL7) in SW480 cells within the co-culture system. (D) Western blot analysis of CSF1 expression in RKO cells with GPSM1 overexpression and knockdown in the co-culture system. (E) ELISA measurement of CSF1 concentration secreted by RKO cells after GPSM1 overexpression or knockdown in the co-culture system. (F) Western blot analysis of CSF1 expression in RKO cells with GPSM1 overexpression and knockdown in the co-culture. (G) ELISA measurement of CSF1 concentration secreted by RKO cells after GPSM1 overexpression or knockdown in the co-culture system. (H) qPCR analysis of M2 macrophage markers (CD206, ARG1, IL-10 and TGF-β) in the co-culture system following CSF1 knockdown in GPSM1-overexpressing RKO cells. (I) qPCR analysis of M2 macrophage markers (CD206, ARG1, IL-10 and TGF-β) in the co-culture system following CSF1 knockdown in GPSM1-overexpressing SW480 cells. (J) Western blot analysis of PD-L1 expression following CSF1 knockdown in GPSM1-overexpressing RKO cells. (K) Western blot analysis of PD-L1 expression following CSF1 knockdown in GPSM1-overexpressing SW480 cells. CRC, colorectal cancer; CSF, colony-stimulating factor. $p < 0.05$; $** p < 0.01$; $*** p < 0.001$. Statistical significance was determined using [insert method, e.g., Student's t-test, ANOVA].

GPSM1 domains based on literature review²⁶ (figure 6H). The results indicated that the GPR domain of GPSM1 was responsible for its interaction with USP9X (figure 6I). Indeed, our additional findings revealed that knockdown of USP9X increased the K63-linked ubiquitination of endogenous GPSM1 (figure 6J).

GPSM1 was a potential therapeutic target for CRC immunotherapy

Given that reduced infiltration of M2-like macrophages has been correlated with the efficacy of immunotherapy in various cancers,^{27,28} we aimed to investigate whether targeting GPSM1 enhances anti-PD1 therapy in CRC. Thus, we screened a library of 87 small-molecule inhibitors that target GPSM1

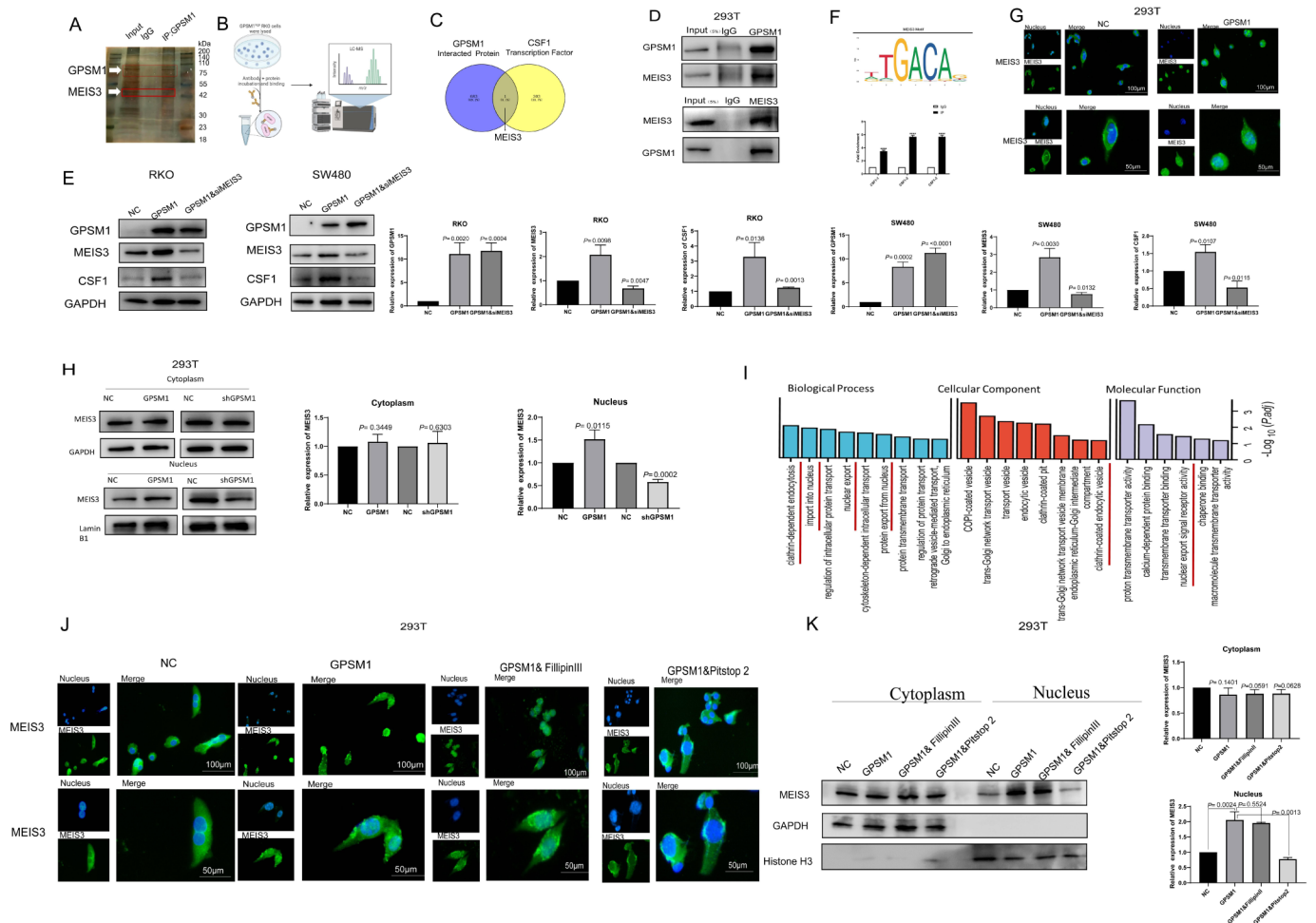
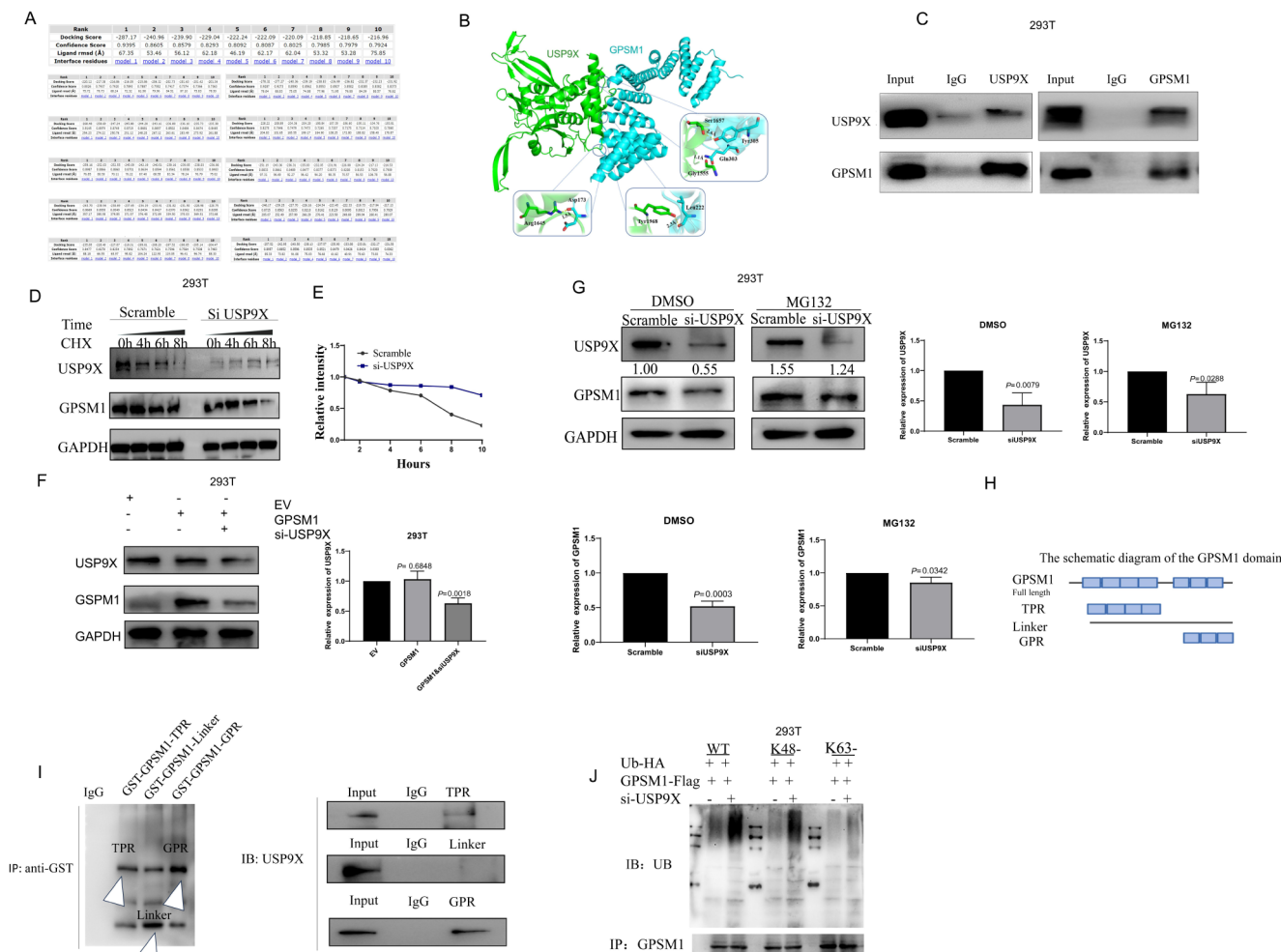


Figure 5 GPSM1 enhances CSF1 expression by promoting the nuclear translocation of MEIS3. (A) The extracted protein was precipitated with anti-GPSM1 antibody and separated by SDS-PAGE, followed by silver staining. (B) Schematic diagram of the IP-MS. (C) Venn diagram of overlapping genes between the GPSM1 binding proteins detected by mass spectrometry and the GSEA transcription factor databases of CSF1. (D) The interaction between GPSM1 and MEIS3 was validated by Co-IP. (E) Western blot analysis of CSF1 expression in GPSM1-overexpressing colorectal cancer cell lines (RKO, SW480) following MEIS3 knockdown. (F) The sequence logo of MEIS3 obtained from the JASPAR website (top). ChIP analysis of MEIS3 for CSF1 promoter regions in HEK293T (bottom). (H) The protein distribution of MEIS3 after nucleoplasmic separation was detected by Western blot. (I) Results from mass spectrometry analysis in a were analyzed for Gene ontology (Go) analyses. (J) HEK293T cells were treated with 5 μ M Pitstop or 10 μ g/mL Filipin III for 15 min, followed by nuclear plasmid separation analysis. (K) HEK293T cells were treated with 5 μ M Pitstop or 10 μ g/mL Filipin III for 15 min, followed by immunofluorescence assay. Scale bars: 100 μ m(top) 50 μ m (bottom). Co-IP, co-immunoprecipitation; CSF, colony-stimulating factor; IP-MS, Immunoprecipitation-Mass Spectrometry.

(figure 7A,online supplemental table S9). The results showed that cell viability in two GPSM1 overexpressing cell lines, RKO and SW480, was reduced by over 50% at a concentration of 2 μ M for rolipram and ruxolitinib (figure 7B,C). Live/dead cell assays further validated an increased number of dead RKO and SW480 cells after ruxolitinib treatment (figure 7E,F). Furthermore, we found that ruxolitinib inhibited the expression of GPSM1 in a dose-dependent and time-dependent manner (figure 7G,H). Using subcutaneous tumor models, we demonstrated that tumor weights in the ruxolitinib-treated group were significantly lower than those in the vehicle group (figure 7I-K). Decreased CD206+cells and increased CD8+cells were shown in the ruxolitinib-treated group compared with

those in the control group (figure 7L-O). We hypothesized that inhibiting GPSM1 by ruxolitinib might enhance the efficacy of anti-PD1 therapy. As expected, we observed that the combination of ruxolitinib and anti-CSF1 with anti-PD1 significantly suppressed the growth of MC38 (MSI-H) syngeneic tumors compared with monotherapies with anti-PD1, ruxolitinib, or anti-CSF1 alone (figure 7P-R). To investigate if targeting the GPSM1 axis could overcome anti-PD1 resistance in MSS CRC, we used a syngeneic CT26 (MSS CRC) tumor model. CT26 cells overexpressing GPSM1 were injected into BALB/C mice, which were then treated with anti-PD1 reagent, ruxolitinib, or BLZ945 (CSF1R inhibitor) (figure 7S-U). Consistent with our previous findings, this combination therapy



effectively suppressed tumor growth in otherwise non-responsive anti-PD1 treated mice. Thus, targeting the GPSM1 pathway not only enhanced the therapeutic efficacy of ICB in MSI-H CRC but also overcame resistance in MSS CRC.

DISCUSSION

Despite the clinical success of ICB, only a small proportion of CRC patients have benefited from anti-PD1 therapy.^{29,30} In the current study, we identified GPSM1, a member of the G-protein signaling regulatory family. Several studies have discovered that GPSM1 can activate inflammatory mediators such as IL-8, which in turn regulates the migration and differentiation of neutrophils

and macrophages.^{31–35} However, the function of GPSM1 in modulating the antitumor immune response remains unclear. Our previous study identified that GPSM1 can inhibit autophagy by activation of the PI3K/AKT/mTOR signaling pathway to promote CRC metastasis.¹¹ In this study, we present novel evidence that deubiquitinase USP9X prevents the degradation of GPSM1 in CRC by deubiquitinating its K63-polyubiquitin chain. This stabilization of GPSM1 leads to the promotion of MEIS3 nuclear translocation, which in turn activates the expression of CSF1. This process induces anti-PD-1 resistance by promoting macrophage polarization towards an immunosuppressive M2 phenotype and enhancing their infiltration into the TME.

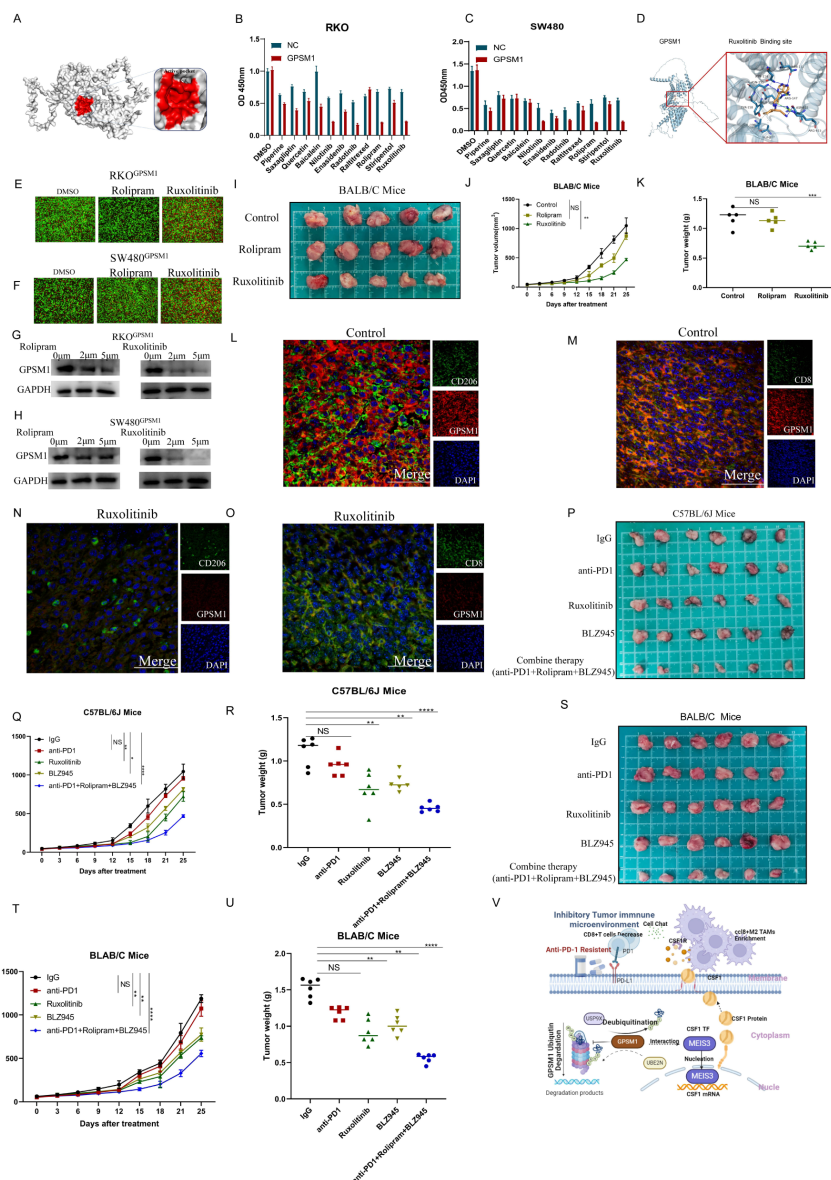


Figure 7 GPSM1 is a potential therapeutic target for CRC immunotherapy. (A) The protein's active sites were determined using the SiteMap module from the Schrödinger software suite, which defines these active sites as docking pockets. (B) A CCK8 assay was performed to evaluate the impact of drugs from the FDA small molecule library on the proliferation of GPSM1-overexpressing RKO cells. (C) A CCK8 assay was performed to evaluate the impact of drugs from the FDA small molecule library on the proliferation of GPSM1-overexpressing SW480 cells. (D) Molecular docking studies were conducted to pinpoint the specific binding sites of ruxolitinib with GPSM1. (E) Live/dead cell staining was performed to evaluate the cytotoxic effects of rolipram and ruxolitinib on GPSM1-overexpressing CRC RKO cells. (F) Live/dead cell staining was performed to evaluate the cytotoxic effects of rolipram and ruxolitinib on GPSM1-overexpressing CRC SW480 cells. (G) Western blot analysis was conducted to investigate the influence of various concentrations of rolipram and ruxolitinib on the expression levels in GPSM1-overexpressing RKO cells alongside their control groups. (H) Western blot analysis was conducted to investigate the influence of various concentrations of rolipram and ruxolitinib on the expression levels in GPSM1-overexpressing SW480 cells alongside their control groups. (I) An in vivo subcutaneous tumorigenesis study in BALB/C Mice was performed to analyze the effects of Rolipram and Ruxolitinib on tumor size and volume. (J, K) Tumor volume and weight were measured at indicated times. (L) Representative IF images of tumor sections in the control group. Green arrows (CD206+cells), red arrows (GPSM1 expression cancer cells). Sarbar: 20 μ m. (M) Representative IF images of tumor sections in the control group. Green arrows (CD8+cells), red arrows (GPSM1 expression cancer cells). Sarbar: 20 μ m. (N) Representative IF images of tumor sections in the ruxolitinib group. Green arrows (CD206+cells), red arrows (GPSM1 expression cancer cells). Sarbar: 20 μ m. (O) Representative IF images of tumor sections in the ruxolitinib group. Green arrows (CD8+cells), red arrows (GPSM1 expression cancer cells). Sarbar: 20 μ m. (P–U) GPSM1 overexpression cells (MC38 and CT26) were subcutaneously injected into C57BL/6 mice and BALB/C mice. When tumors reached 80–130 mm^3 , mice were treated with anti-PD1, ruxolitinib, BLZ945, or a combination. Tumor volumes and weights were measured at indicated times. (V) Schematic diagram of the article. CRC, colorectal cancer. $p < 0.05$; $** p < 0.01$; $*** p < 0.001$; $**** p < 0.0001$. Statistical significance was determined using [insert method, e.g., Student's t-test, ANOVA].

As the predominant immune cells in the TME, TAMs play a crucial role in enabling cancers to evade immune surveillance.³⁶ Elucidating the mechanisms underlying macrophage recruitment and M2-like polarization may provide valuable insights into potential drug combination strategies to enhance the efficacy of anti-PD-1 therapy in CRC. It is well known that CSF1 interacts with its receptor, CSF1R, to control macrophage migration, proliferation, and polarization.³⁷ Wei *et al* demonstrated that macrophage-secreted CSF1 drives anti-PD1 tolerance in hepatocellular carcinoma (HCC) by ZFP64.³⁸ Similarly, Ying *et al* found that OPN promotes PD-L1 expression in HCC via activation of the CSF1-CSF1R pathway in macrophages.³⁹ In this study, we found that high GPSM1 expression in CRC was associated with reduced immune cell infiltration within the tumor and an increased likelihood of treatment resistance. However, due to challenges in obtaining biopsy samples and the limited sample size, the conclusions of this experiment require further validation through additional studies with larger cohorts. Additionally, we demonstrated that GPSM1 promotes the transcriptional upregulation of CSF1 by facilitating the nuclear translocation of MEIS3. Following this, *in vitro* co-culture experiments with GPSM1 overexpression CRC cells and macrophages demonstrated that the secreted CSF1 significantly encouraged M2 polarization of the recruited macrophages. This process subsequently established an immunosuppressive TME and played a role in the resistance to anti-PD-1 therapy in CRC.

The ubiquitin-proteasome system primarily governs intracellular protein degradation and turnover.⁴⁰ When this system becomes dysregulated, it can lead to the overexpression of oncoproteins or the downregulation of tumor suppressors, ultimately causing tumorigenesis.⁴¹ Our current evidence indicates that GPSM1 may act as an oncoprotein, though the upstream regulatory mechanisms remain unclear. Previous studies have shown that the deubiquitinase USP9X regulates GPSM1 expression.²⁵ In our research, we identified that USP9X is highly expressed and positively correlated with GPSM1 expression. Additionally, we uncovered that USP9X stabilizes GPSM1 by regulating K63-linked polyubiquitin chains, thus increasing GPSM1 expression in CRC.

Given the lack of commercially available drugs that target GPSM1, we employed a small-molecule compound library to discover and evaluate inhibitors of GPSM1 expression. Ruxolitinib emerged as one of these identified inhibitors, and it has previously demonstrated the ability to attenuate the progression of various tumors.^{42–44} Jashodeep *et al* show that ruxolitinib could reprogram the cancer-associated fibroblast to overcome resistance to immune checkpoint inhibition in pancreatic ductal adenocarcinoma.⁴² Our study found that ruxolitinib significantly inhibited the growth of subcutaneous tumors in mice with high GPSM1 expression. More importantly, we discovered that the combination therapy of ruxolitinib with anti-PD1 and CSF1 inhibitors reduced tumor size

and reversed anti-PD1 resistance in both MSI and MSS mice tumor models.

In conclusion, our study revealed that the USP9X/GPSM1/CSF1 axis induces an immunosuppressive microenvironment enriched with M2 macrophages, which is a key reason for the resistance of CRC patients to anti-PD-1 therapy. Moreover, we found that the combination therapy of ruxolitinib and anti-PD1 can overcome this immunosuppressive microenvironment, enhancing the efficacy of anti-PD1 treatment in both MSI and MSS types of CRC. This provides a potential therapeutic strategy for precision medicine based on GPSM1 expression levels to develop combined anti-PD1 treatments.

Acknowledgments We sincerely thank Professor Zhizhang Yang from Mayo Clinic for his invaluable assistance in improving the language of the revised manuscript.

Contributors YC contributed to data curation, software development, formal analysis, investigation, visualization, methodology, and drafting of the original manuscript. HJ and XZ were responsible for validation, methodology, and software development. HZ and YX conducted investigations. YY contributed to the methodology. NL was responsible for validation. XX conceptualized and supervised the study, acquired funding, managed the project, and contributed to drafting the original manuscript as well as reviewing and editing the final version. Guarantor XX serves as the guarantor of this work, accepting full responsibility for the integrity of the data and the accuracy of the analysis.

Funding This work was supported by the National Natural Science Foundation of China, Joint Foundation Programs (U23A20418), Qingdao Municipal Science and Technology Bureau Municipal Science (23-2-8-smjk-19-nsh).

Competing interests None declared.

Patient consent for publication Not applicable.

Ethics approval This study was approved by the Ethics Committee of The Affiliated Hospital of Qingdao University (Approval No. QYFYW2LL29213) and Medical and Experimental Animal Ethics Committee of The Affiliated Hospital of Qingdao University (Approval No. AHQU-MAL20240531LN). All participants provided written informed consent. All experiments were carried out in accordance with the Code of Ethics of the World Medical Association (Declaration of Helsinki).

Provenance and peer review Not commissioned; externally peer reviewed.

Data availability statement Data are available in a public, open access repository. Data are available on reasonable request. The raw scRNA sequencing reads generated in this study have been deposited in the CNGB database, Bioproject accession number: CNP0006600. The data are available on reasonable request. All relevant data are included in the article or uploaded as supplementary information. The datasets used and/or analyzed during this study can be accessed from the corresponding author on reasonable request.

Supplemental material This content has been supplied by the author(s). It has not been vetted by BMJ Publishing Group Limited (BMJ) and may not have been peer-reviewed. Any opinions or recommendations discussed are solely those of the author(s) and are not endorsed by BMJ. BMJ disclaims all liability and responsibility arising from any reliance placed on the content. Where the content includes any translated material, BMJ does not warrant the accuracy and reliability of the translations (including but not limited to local regulations, clinical guidelines, terminology, drug names and drug dosages), and is not responsible for any error and/or omissions arising from translation and adaptation or otherwise.

Open access This is an open access article distributed in accordance with the Creative Commons Attribution Non Commercial (CC BY-NC 4.0) license, which permits others to distribute, remix, adapt, build upon this work non-commercially, and license their derivative works on different terms, provided the original work is properly cited, appropriate credit is given, any changes made indicated, and the use is non-commercial. See <http://creativecommons.org/licenses/by-nc/4.0/>.

ORCID iD

Yang Chen <http://orcid.org/0009-0000-5982-2082>

REFERENCES

- 1 Dekker E, Tanis PJ, Vleugels JLA, *et al.* Colorectal cancer. *The Lancet* 2019;394:1467–80.
- 2 Ganesh K, Stadler ZK, Cercek A, *et al.* Immunotherapy in colorectal cancer: rationale, challenges and potential. *Nat Rev Gastroenterol Hepatol* 2019;16:361–75.
- 3 Ganesh K. Optimizing immunotherapy for colorectal cancer. *Nat Rev Gastroenterol Hepatol* 2022;19:93–4.
- 4 Kubli SP, Berger T, Araujo DV, *et al.* Beyond immune checkpoint blockade: emerging immunological strategies. *Nat Rev Drug Discov* 2021;20:899–919.
- 5 Li J, Wu C, Hu H, *et al.* Remodeling of the immune and stromal cell compartment by PD-1 blockade in mismatch repair-deficient colorectal cancer. *Cancer Cell* 2023;41:1152–69.
- 6 Sui Q, Zhang X, Chen C, *et al.* Inflammation promotes resistance to immune checkpoint inhibitors in high microsatellite instability colorectal cancer. *Nat Commun* 2022;13:7316.
- 7 Blumer JB, Cismowski MJ, Sato M, *et al.* AGS proteins: receptor-independent activators of G-protein signaling. *Trends Pharmacol Sci* 2005;26:470–6.
- 8 Adekoya TO, Smith N, Aladeniyi T, *et al.* Activator of G protein signaling 3 modulates prostate tumor development and progression. *Carcinogenesis* 2019;40:1504–13.
- 9 Zhang Y, Zhou B, Sun J, *et al.* Knockdown of GPSM1 Inhibits the Proliferation and Promotes the Apoptosis of B-Cell Acute Lymphoblastic Leukemia Cells by Suppressing the ADCY6-RAPGEF3-JNK Signaling Pathway. *Pathol Oncol Res* 2021;27:643376.
- 10 Shi H, Ren H, Yang X, *et al.* Overexpression of activator of G-protein signaling 3 decreases the proliferation of esophageal squamous cell carcinoma. *Pathol Res Pract* 2015;211:449–55.
- 11 Yang C, Yaolin S, Lu W, *et al.* G-protein signaling modulator 1 promotes colorectal cancer metastasis by PI3K/AKT/mTOR signaling and autophagy. *Int J Biochem Cell Biol* 2023;157:106388.
- 12 Wu VH, Yung BS, Faraji F, *et al.* The GPCR-Gq_s-PKA signaling axis promotes T cell dysfunction and cancer immunotherapy failure. *Nat Immunol* 2023;24:1318–30.
- 13 Huang D, Chen X, Zeng X, *et al.* Targeting regulator of G protein signaling 1 in tumor-specific T cells enhances their trafficking to breast cancer. *Nat Immunol* 2021;22:865–79.
- 14 Chen D, Zhang X, Li Z, *et al.* Metabolic regulatory crosstalk between tumor microenvironment and tumor-associated macrophages. *Theranostics* 2021;11:1016–30.
- 15 Wei C, Yang C, Wang S, *et al.* Crosstalk between cancer cells and tumor associated macrophages is required for mesenchymal circulating tumor cell-mediated colorectal cancer metastasis. *Mol Cancer* 2019;18:64.
- 16 Mantovani A, Marchesi F, Jaillon S, *et al.* Tumor-associated myeloid cells: diversity and therapeutic targeting. *Cell Mol Immunol* 2021;18:566–78.
- 17 Pittet MJ, Michielin O, Migliorini D. Clinical relevance of tumour-associated macrophages. *Nat Rev Clin Oncol* 2022;19:402–21.
- 18 Sunakawa Y, Stintzing S, Cao S, *et al.* Variations in genes regulating tumor-associated macrophages (TAMs) to predict outcomes of bevacizumab-based treatment in patients with metastatic colorectal cancer: results from TRIBE and FIRE3 trials. *Ann Oncol* 2015;26:2450–6.
- 19 Yang C, Qing J, Yan Z, *et al.* Data from: disruption of GPSM1/CSF1 signaling reprograms tumor-associated macrophages to overcome Anti-PD-1 resistance in colorectal cancer. China National Gene Bank; 2024. Available: <https://db.cngb.org/search/project/CNP0006600/>
- 20 Liu T, Fu J, Zeng Z, *et al.* Data from: TIMER2.0 for analysis of tumor-infiltrating immune cells [TIMER2.0]. 2020. Available: <http://timer.cistrome.org>
- 21 Choe S-K, Lu P, Nakamura M, *et al.* Meis cofactors control HDAC and CBP accessibility at Hox-regulated promoters during zebrafish embryogenesis. *Dev Cell* 2009;17:561–7.
- 22 Vlachakis N, Choe SK, Sagerström CG. Meis3 synergizes with Pbx4 and Hoxb1b in promoting hindbrain fates in the zebrafish. *Development* 2001;128:1299–312.
- 23 Locatelli P, Belaich MN, López AE, *et al.* Novel insights into cardiac regeneration based on differential fetal and adult ovine heart transcriptomic analysis. *Am J Physiol Heart Circ Physiol* 2020;318:H994–1007.
- 24 Liu J, Wang Y, Birnbaum MJ, *et al.* Three-amino-acid-loop-extension homeodomain factor Meis3 regulates cell survival via PDK1. *Proc Natl Acad Sci USA* 2010;107:20494–9.
- 25 Xu Z, Xia B, Gong Q, *et al.* Identification of a deubiquitinating enzyme as a novel AGS3-interacting protein. *PLoS One* 2010;5:e9725.
- 26 De Vries L, Fischer T, Tronchère H, *et al.* Activator of G protein signaling 3 is a guanine dissociation inhibitor for Gα_i subunits. *Proc Natl Acad Sci U S A* 2000;97:14364–9.
- 27 Braun DA, Street K, Burke KP, *et al.* Progressive immune dysfunction with advancing disease stage in renal cell carcinoma. *Cancer Cell* 2021;39:632–48.
- 28 Zhang X, Wei Z, Yong T, *et al.* Cell microparticles loaded with tumor antigen and resiquimod reprogram tumor-associated macrophages and promote stem-like CD8⁺ T cells to boost anti-PD-1 therapy. *Nat Commun* 2023;14:5653.
- 29 Bortolomeazzi M, Keddar MR, Montorsi L, *et al.* Immunogenomics of Colorectal Cancer Response to Checkpoint Blockade: Analysis of the KEYNOTE 177 Trial and Validation Cohorts. *Gastroenterology* 2021;161:1179–93.
- 30 Chen X, Jia M, Ji J, *et al.* Exosome-Derived Non-Coding RNAs in the Tumor Microenvironment of Colorectal Cancer: Possible Functions, Mechanisms and Clinical Applications. *Front Oncol* 2022;12:887532.
- 31 Blumer JB, Chandler LJ, Lanier SM. Expression analysis and subcellular distribution of the two G-protein regulators AGS3 and LGN indicate distinct functionality. Localization of LGN to the midbody during cytokinesis. *J Biol Chem* 2002;277:15897–903.
- 32 Choi I-W, Ahn DW, Choi J-K, *et al.* Regulation of Airway Inflammation by G-protein Regulatory Motif Peptides of AGS3 protein. *Sci Rep* 2016;6:27054.
- 33 Branham-O'Connor M, Robichaux WG III, Zhang X-K, *et al.* Defective Chemokine Signal Integration in Leukocytes Lacking Activator of G Protein Signaling 3 (AGS3). *Journal of Biological Chemistry* 2014;289:10738–47.
- 34 Yan J, Zhang Y, Yu H, *et al.* GPSM1 impairs metabolic homeostasis by controlling a pro-inflammatory pathway in macrophages. *Nat Commun* 2022;13:7260.
- 35 Singh V, Raghuwanshi SK, Smith N, *et al.* G Protein-coupled receptor kinase-6 interacts with activator of G protein signaling-3 to regulate CXCR2-mediated cellular functions. *J Immunol* 2014;192:2186–94.
- 36 Chen S, Saeed AFUH, Liu Q, *et al.* Macrophages in immunoregulation and therapeutics. *Signal Transduct Target Ther* 2023;8:207.
- 37 Hume DA, MacDonald KPA. Therapeutic applications of macrophage colony-stimulating factor-1 (CSF-1) and antagonists of CSF-1 receptor (CSF-1R) signaling. *Blood* 2012;119:1810–20.
- 38 Wei C-Y, Zhu M-X, Zhang P-F, *et al.* PKCα/ZFP64/CSF1 axis resets the tumor microenvironment and fuels anti-PD1 resistance in hepatocellular carcinoma. *J Hepatol* 2022;77:163–76.
- 39 Zhu Y, Yang J, Xu D, *et al.* Disruption of tumour-associated macrophage trafficking by the osteopontin-induced colony-stimulating factor-1 signalling sensitises hepatocellular carcinoma to anti-PD-L1 blockade. *Gut* 2019;68:1653–66.
- 40 Pohl C, Dikic I. Cellular quality control by the ubiquitin-proteasome system and autophagy. *Science* 2019;366:818–22.
- 41 Cui Z, Cong M, Yin S, *et al.* Role of protein degradation systems in colorectal cancer. *Cell Death Discov* 2024;10:141.
- 42 Datta J, Dai X, Bianchi A, *et al.* Combined MEK and STAT3 Inhibition Uncovers Stromal Plasticity by Enriching for Cancer-Associated Fibroblasts With Mesenchymal Stem Cell-Like Features to Overcome Immunotherapy Resistance in Pancreatic Cancer. *Gastroenterology* 2022;163:1593–612.
- 43 Ruxolitinib Benefits Some with Pancreatic Cancer. *Cancer Discov* 2015;5:1231.
- 44 Qureshy Z, Li H, Zeng Y, *et al.* STAT3 Activation as a Predictive Biomarker for Ruxolitinib Response in Head and Neck Cancer. *Clin Cancer Res* 2022;28:4737–46.